

Thermopower in the Ba 1–δ M 2+x Ru 4–x O 11 (M = Co, Mn, Fe) magnetic hexagonal ruthenates

Florent Pawula, Ramzy Daou, Sylvie Hébert, D. Pelloquin, Jean Juraszek, Antoine Maignan

▶ **To cite this version:**

Florent Pawula, Ramzy Daou, Sylvie Hébert, D. Pelloquin, Jean Juraszek, et al.. Thermopower in the Ba 1–δ M 2+x Ru 4–x O 11 (M = Co, Mn, Fe) magnetic hexagonal ruthenates. Physical Review B, 2021, 103 (23), pp.235106. 10.1103/PhysRevB.103.235106 . hal-03447165

HAL Id: hal-03447165
https://hal.science/hal-03447165

Submitted on 24 Nov 2021

HAL is a multi-disciplinary open access archive for the deposit and dissemination of scientific research documents, whether they are published or not. The documents may come from teaching and research institutions in France or abroad, or from public or private research centers.

L'archive ouverte pluridisciplinaire **HAL**, est destinée au dépôt et à la diffusion de documents scientifiques de niveau recherche, publiés ou non, émanant des établissements d'enseignement et de recherche français ou étrangers, des laboratoires publics ou privés.

Thermopower in the $Ba_{1-\delta}M_{2+x}Ru_{4-x}O_{11}$ (M = Co, Mn, Fe) magnetic hexagonal ruthenates

Florent Pawula,[1] Ramzy Daou,[1] Sylvie Hébert,[1,*] Denis Pelloquin,[1] Jean Juraszek,[2] and Antoine Maignan[1]
[1]*Normandie Univ, ENSICAEN, UNICAEN, CNRS, CRISMAT, 14000 Caen, France*
[2]*Normandie Univ, UNIROUEN, INSA Rouen, CNRS, GPM, 76000 Rouen, France*

(Received 12 June 2020; revised 16 February 2021; accepted 29 April 2021; published xxxxxxxxxx)

The magnetism, magnetotransport, and Seebeck coefficients (S) for three ruthenates $Ba_{1-\delta}M_{2+x}Ru_{4-x}O_{11}$ ($\delta = 0.06$; M = Mn, Co; $x = 0.4$) and $Sr_{1-\delta}M_{2+x}Ru_{4-x}O_{11}$ ($\delta = 0.02$; M = Fe; $x = 0.7$) compositions have been studied. Their crystallographic structures contain three metal sites, edge-sharing octahedra forming kagome lattices, face-shared octahedra with the shortest Ru(M)-Ru(M) distance, and MO_5 trigonal bipyramids. These three compositions have been selected for their transport behavior exhibiting small resistivity values (∼mΩ cm) together with a complex ferrimagnetic behavior, with localization increasing from M = Co to M = Fe. This enabled the thermopower to be measured in hexagonal ruthenates in which the conducting kagome layers are more or less diluted by three different magnetic cations substituted for Ru. The positive Seebeck coefficient of the three compounds is found to increase up to 750 K to values in the range of 22 to 35 μV K^{-1}. Such values, similar to those of perovskite ruthenates, reveal a Seebeck coefficient dominated by the Ru network at high temperature whatever the foreign magnetic cation is. In addition, below about 50 K, the values of S are very small for M = Mn and Co, and the $S(T)$ curves of the $Ba_{1-\delta}M_{2.4}Ru_{3.6}O_{11}$ compounds exhibit similarities with that of ruthenium metal. This is interpreted by shorter Ru-Ru distances as compared with perovskite ruthenates allowing a metallic direct exchange. The ferrimagnetism associated with the M cation does not seem to play a major role in transport, as there is almost no impact of the magnetic ordering on thermopower and electrical resistivity and the values of magnetoresistance remain very small, reaching at most −1% in 9 T at 5 K for M = Mn, and −0.4% at T_C for M = Co. The present results obtained in these phases containing hexagonal Ru networks show that Hund's metal model developed to describe the thermopower of perovskite ruthenates with a Ru square lattice can have a broader range of validity.

DOI: 10.1103/PhysRevB.00.005100

I. INTRODUCTION

Compared to 3d oxides, the ruthenates with structures derived from the perovskites possess an extra degree of freedom with spin-orbit coupling which can generate unique properties. Electronic and magnetic properties can be strongly modified in these ruthenium oxides, depending on the crystallographic structure, where 3D or 2D layers have more or less tilted RuO_6 octahedra. Among the most investigated properties, superconductivity and strong magnetic fluctuations in Sr_2RuO_4 [1,2], and a transition from paramagnetism (PM) to ferromagnetism (FM) when going from $CaRuO_3$ to $SrRuO_3$ metallic perovskites have been studied in detail [3–6]. Interestingly, the thermopower in these ruthenates has been reported to exhibit a nontrivial behavior with positive values, increasing up to high T and reaching a value close to +20–30 μV K^{-1} at $T \gg 300$ K, independently of the transport and magnetic properties [7–10]. More recently, the intriguing transport properties of Sr_2RuO_4 have been interpreted considering the possible existence of resilient quasiparticles [11,12]. In Ref. [12], the dominant role at high T of Ru spin entropy on the Seebeck coefficient of Sr_2RuO_4 has been evidenced, the spins remaining unquenched at a decoherence T much smaller than that of the orbital degrees of freedom [12]. In this model, for tetravalent Ru in structures deriving from the perovskite, solely the $4d^3$ (hole) and $4d^5$ (electron) spin degeneracies have to be taken into account at high T, explaining the intriguing constant values all close to 30 μV K^{-1}.

Apart from these square lattices of Ru^{4+}, much less is known about the thermopower in ruthenates with other structural types such as hexagonal. Among the latter, the $A_{1-\delta}M_{2+x}Ru_{4-x}O_{11}$ "124" oxides (A = Ba, Sr; M = Co, Mn, Fe, Cu, Li, Zn, Ni and with $-1 < x < 1.5$) exhibit interesting properties [13–20] but with a more complex crystallographic structure, the elementary lattice being a stacking of two layers deriving from "R-type" blocks, isotypic to (K, Na, Sr, Pb)V_6O_{11} magnetoplumbite [21,22]. Three different crystallographic sites coexist (Fig. 1): a 2D layer with a kagome lattice (6g sites), interconnected by two face-shared octahedra (4e sites) and trigonal bipyramids (2d sites). For $A_{1-\delta}M_{2+x}Ru_{4-x}O_{11}$ ($x \neq -1$) the kagome lattice and face-shared octahedra present mixed occupation by Ru and M cations, while the bipyramids are nearly 100% occupied by M [14–16,23,24]. On the other hand, in $BaZnRu_5O_{11}$, $BaLiRu_5O_{11}$, or $BaCu_{1+x}Ru_{5-x}O_{11}$, the face-shared 4e site is fully occupied by Ru [14,17,25]. The valencies determined from x-ray diffraction and charge-balance calculations are reported to be Mn^{3+} [14], Co^{2+} or Fe^{2+}/Fe^{3+}, and Ru^{3+}/Ru^{5+} [25]. In $BaMRu_5O_{11}$, the face-shared site contains Ru^{4+} calculated from bond valence sum while the valency is closer to 3.8 in the kagome lattice [14], and recent x-ray absorption

*sylvie.hebert@ensicaen.fr

 ©2021 American Physical Society

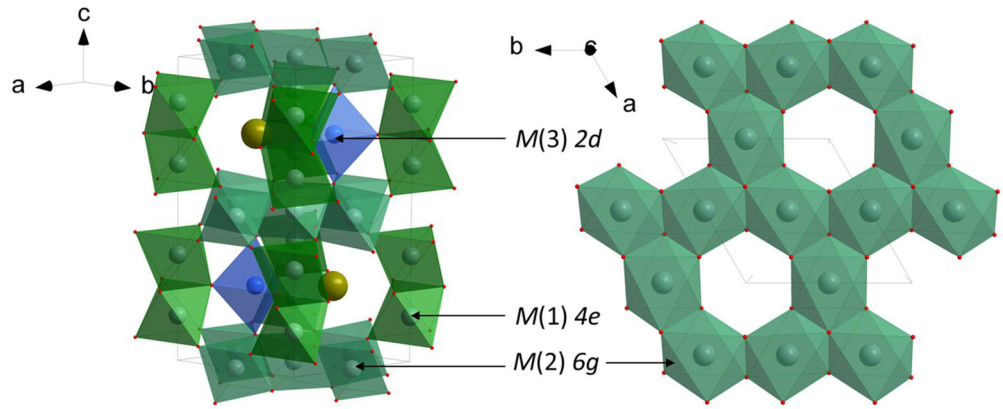


FIG. 1. $AM_{2\pm x}Ru_{4\mp x}O_{11}$ structure of $P6_3/mmc$ space group with A alkaline-earth (yellow) in $2a$ sites, $2d$ trigonal bipyramid sites $M(3)O_5$ (blue), $4e$ face-shared octahedra sites $M(1)_2O_9$ (green), and $6g$ edge-shared octahedra sites $M(2)O_6$ forming a kagome network as illustrated in plan [001] (right).

spectroscopy experiments have found that Ru mean valency is close to 3.8 for $BaCu_{1+x}Ru_{5-x}O_{11}$, with Cu being dominantly 2+ [17].

These materials present a rich variety of properties with frustrated magnetism arising from the kagome lattice as reported in $BaZnRu_5O_{11}$ [18], in $SrNiRu_5O_{11}$ [20], or in $SrSn_2Ga_{1.3}Cr_{2.7}O_{11}$ [26], and possible spintronic applications for metallic and ferrimagnetic materials in $SrCo_{1.89}Ru_{4.11}O_{11}$ [16] or in $BaFe_{2\pm x}Ru_{4\mp x}O_{11}$ [27]. The complex magnetic structure of $BaFe_{2\pm x}Ru_{4\mp x}O_{11}$ with spin chirality in the kagome planes leads to a strong anomalous Hall effect [27]. Also, a possible topological insulator state has been discussed in $SrNiRu_5O_{11}$ due to the nonconventional temperature dependence of specific heat [20].

For $M =$ Co and $M =$ Mn in $A_{1-\delta}M_{2+x}Ru_{4-x}O_{11}$, these materials are metallic and present ferromagnetic-like magnetization loops [14,24] with a very small coercive field and have thus been considered as good candidates for spintronic applications. Their magnetic structures strongly depend on the magnetic $3d$ M element, with the easy axis perpendicular to the kagome lattice for $M =$ Mn ($BaMn_2Ru_4O_{11}$) [14] and $M =$ Fe ($SrFe_{3.26}Ru_{2.74}O_{11}$) [28], or parallel to it for $M =$ Co ($BaCo_{1.68}Ru_{4.32}O_{11}$) [28]. Neutron diffraction refinements for $M =$ Mn, Co have demonstrated a lack of magnetic moment in the face-shared octahedra, but magnetic moments coming only from M in the two other sites, the Ru cations bearing no magnetic moments [14]. This unexpected lack of moment has also been reported in $BaCu_{1+x}Ru_{5-x}O_{11}$ and may be related to a $J = 0$ state of Ru^{4+} induced by distortion within the kagome lattice [17]. The magnetism in $BaMn_2Ru_4O_{11}$, $SrFe_{3.26}Ru_{2.74}O_{11}$, and $BaCo_{1.68}Ru_{4.32}O_{11}$ comes thus from a complex combination of moments diluted on a kagome lattice, and moments in the trigonal bipyramids. For $M =$ Fe, the three sites are magnetic, with ferromagnetic moments for the $2d$ and $6g$ sites, these moments being antiferromagnetically coupled to the $4e$ site (face-shared octahedra). Similarly, the electrical resistivity strongly depends on M, being more or less localized (electrical resistivity increasing from $M =$ Co to Mn and Fe) and the Hall coefficient is characteristic of n-type doping for $M =$ Co in $SrCo_2Ru_4O_{11}$, but p-type doping for $M =$ Fe in $BaFe_{3.4}Ru_{2.6}O_{11}$ single crystals [25]. Thus, this "124" family constitutes a rich playground to study the thermopower in hexagonal systems which resistivity and magnetism can be modified by changing the M cation, and/or the M/Ru ratio. Even if the complex crystallographic structure with several cationic environments and mixed occupancies precludes a complete understanding of the transport properties, the comparison of the properties of different selected M transition cations can give interesting information on the respective roles of Ru and M. We have therefore selected $BaCo_2Ru_4O_{11}$, $BaMn_2Ru_4O_{11}$, and $SrFe_2Ru_4O_{11}$ for their metal-like ($d\rho/dT > 0$) to more localized transport properties ($d\rho/dT < 0$) and for their soft ferromagnetic to hard ferrimagnetic properties, respectively. Considering the dominant role of Ru spin entropy in the thermopower of perovskite and quadruple perovskite ruthenates at high T, the Seebeck coefficient of these 124 oxides has been studied up to 750 K. Also, to explain the low-T metallic thermopower, the Seebeck coefficient of pure ruthenium has been measured. In the following, we report the thermopower, resistivity, and magnetism of these hexagonal ruthenates to study the role of both magnetic ordering on and ruthenium spin entropic contribution to the thermopower.

II. EXPERIMENT

Polycrystalline samples of $BaCo_2Ru_4O_{11}$, $BaMn_2Ru_4O_{11}$, and $SrFe_2Ru_4O_{11}$ nominal compositions were synthesized by solid-state reaction. Stoichiometric amounts of $1g$ for $BaO{:}RuO_2{:}CoO_{1.32}$:Co metal = 1:4:3/2:1/2, $BaO{:}RuO_2{:}$MnO = 1:4:2, and $SrO{:}RuO_2{:}Fe_2O_3$:Fe metal = 1:4:2/3:2/3 were ground during 15 min in an agate mortar before being pressed into bar shape. Bars introduced in Al_2O_3 crucibles were sealed in silica tubes under primary vacuum. These tubes were sintered at 1050 °C for 12 h then 24 h at 175 °C/h for the cobalt and iron compounds; and 1125 °C for 24 h at 93.75 °C/h for the manganese compound. To compare these 124 oxides with pure ruthenium metal, a ruthenium sample has been shaped from Ru metal powder (Alfa Aesar 99.9%, −325 mesh) using an arc furnace.

The x-ray powder-diffraction patterns were recorded at room temperature using a standard powder diffractometer X'PERT Pro PANalytical in θ-2θ mode. Two specific wavelengths have been applied: Cu Kα radiation for Co,

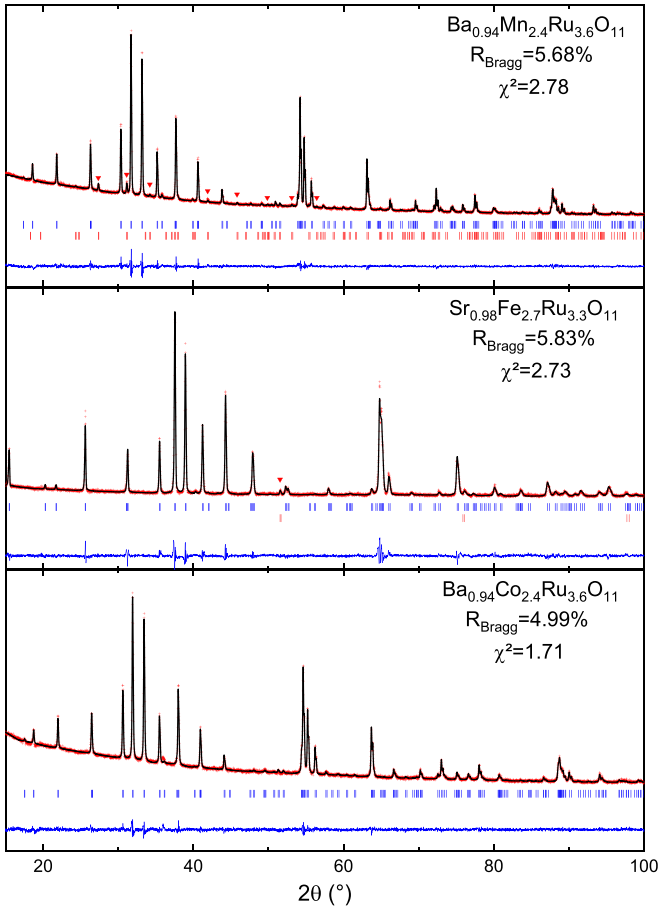


FIG. 2. Rietveld refinement of $Ba_{0.94}Mn_{2.4}Ru_{3.6}O_{11}$ (upper panel), $Sr_{0.98}Fe_{2.7}Ru_{3.3}O_{11}$ (middle panel), and $Ba_{0.94}Co_{2.4}Ru_{3.6}O_{11}$ (bottom panel) with their respective quality factor. Red crosses are experimental data, black lines are calculated fits, and blue lines are the differences between fits and data. Note the presence of $BaRuO_3$ (red triangles) as impurity in $Ba_{0.94}Mn_{2.4}Ru_{3.6}O_{11}$, and Fe (red triangles) in $Sr_{0.98}Fe_{2.7}Ru_{3.3}O_{11}$.

Mn-based ruthenates and Co Kα radiation for Fe-based ruthenate. Powder-diffraction patterns were refined by the Rietveld method with the FULLPROF software implemented in the WINPLOTR package [29].

The samples' purity and chemical homogeneity have been probed by (scanning) transmission electron microscopy ((S)TEM) techniques. This work has been jointly performed with an FEI TECNAI 30UT ($Cs = 0.7$ mm) working at 300 kV and a JEOL ARM200 cold FEG double-corrected microscope, equipped with an energy dispersive x-ray (EDX) analyzer. Complementary simulated images have been calculated with the JEMS software [30].

Magnetic property measurements were performed using either a 5 T superconducting quantum interference device magnetometer (Quantum Design) from 2 to 400 K or the AC Measurement System option of a 14 T Physical Properties Measurement System (PPMS, Quantum Design) from 5 to 350 K. Electrical resistivities were measured with a four-probe method with copper wires and indium contacts using the transport option of a 9 T PPMS from 5 to 400 K. Magnetoresistance was also measured at different temperatures and up to

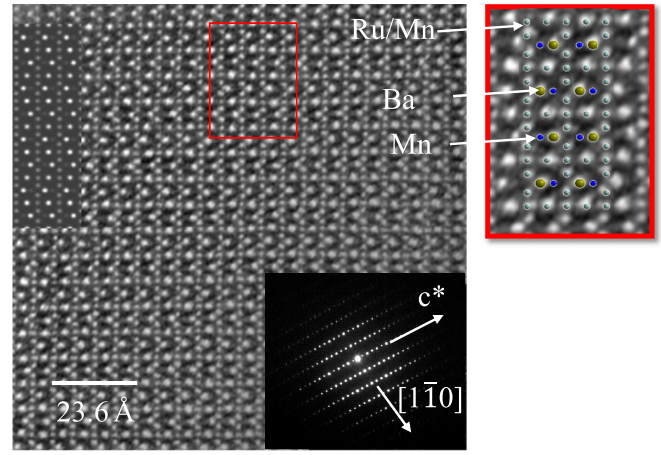


FIG. 3. Crystal model and STEM ADF image of $Ba_{0.94}Mn_{2.4}Ru_{3.6}O_{11}$ (left panel) with ED pattern (left panel bottom inset), simulation (left panel upper inset), and superposition of the crystallographic structure extracted from Rietveld refinements with atom in color (gray: Ru/Mn in 4*e* and 6*g* sites, blue: Mn in 2*d* sites, and yellow Ba in 2*a* sites).

9 T in the same configuration and apparatus. Thermoelectric properties were studied using both homemade apparatus (steady-state technique) with indium contacts and the PPMS Thermal Transport Option with silver epoxy contacts, both options being used in a 9 T PPMS from 2 to 390 K. High-temperature Seebeck coefficient and resistivity were probed with a Seebeck Coefficient/Electrical Resistance Measuring System (ZEM-3, ULVAC) from 300 to 775 K.

The low-temperature thermopower of metallic Ru was measured in the 8 K $< T <$ 150 K temperature range using a standard steady-state one-heater two-thermometer technique. The temperature difference across the samples was measured using chromel/phosphor-bronze thermocouples attached with Dupont 4929N silver paste. The thermoelectric voltage was measured with reference to the phosphor-bronze leads. In this temperature range the contribution of these leads to the signal is negligible ($<$50 nV K^{-1}) and has not been subtracted from the data [31].

^{57}Fe Mössbauer measurements were carried out in transmission geometry at 300 and 20 K. A ^{57}Co in Rh matrix radioactive source of ∼1.5 GBq activity was employed in constant acceleration mode. The spectra were fitted with the MOSFIT code using the histogram method and Lorentzian lines. Isomer shifts are given with respect to α-Fe at 300 K.

III. RESULTS AND DISCUSSION

A. Structural analyses

The x-ray powder diffractograms of the three samples (Fig. 2) can be indexed in hexagonal cell with the centrosymmetric space group, characteristic of 124 ferrite. This structural filiation is confirmed by the electron microscopy studies especially from the atomic STEM micrographs recorded with an annular dark-field (ADF) detector and their electronic diffraction (ED). Simulations have also been calculated from atomic positions deduced from the Rietveld analysis and superimposed on the experimental

TABLE I. Atom occupations from Rietveld refinement with uncertainty between parentheses.

	$Ba_{0.94(1)}Mn_{2.44(7)}Ru_{3.56(7)}O_{11}$		$Ba_{0.94(1)}Co_{2.43(7)}Ru_{3.57(7)}O_{11}$		$Sr_{0.98(1)}Fe_{2.66(4)}Ru_{3.34(4)}O_{11}$	
Site	Atom	Occ. (%)	Atom	Occ. (%)	Atom	Occ. (%)
2*a*	Ba	94(1)	Ba	94(1)	Sr	98(1)
4*e*	Mn1	24(2)	Co1	22(2)	Fe1	45(1)
	Ru1	76(2)	Ru1	78(2)	Ru1	55(1)
6*g*	Mn2	32(1)	Co2	32(1)	Fe2	26(1)
	Ru2	68(1)	Ru2	68(1)	Ru2	74(1)
2*d*	Mn3	100	Co3	100	Fe3	100

micrograph as shown in Fig. 3. The x-ray diffraction (XRD) study reveals also the purity of $BaCo_2Ru_4O_{11}$ sample in contrast to $BaMn_2Ru_4O_{11}$ and $SrFe_2Ru_4O_{11}$ samples where the presence of extra peaks on the pattern has been detected, revealing small amount of $BaRuO_3$ (3 wt.%) and Fe (0.02 wt.%), respectively. Refined cell parameters are $a = 5.8882(3)$ Å and $c = 13.5489(1)$ Å for $BaMn_2Ru_4O_{11}$, $a = 5.8399(1)$ Å, and $c = 13.4745(3)$ Å for $BaCo_2Ru_4O_{11}$, and $a = 5.8695(1)$ Å and $c = 13.2883(2)$ Å for $SrFe_2Ru_4O_{11}$, consistent with previous reports [14,16,32]. With those parameters, fixing the oxygen occupancy to 11 and assuming full metal site occupations, the structural Rietveld refinements lead to $Ba_{0.94(1)}Co_{2.43(7)}Ru_{3.57(7)}O_{11}$, $Ba_{0.94(1)}Mn_{2.44(7)}Ru_{3.56(7)}O_{11}$, and $Sr_{0.98(1)}Fe_{2.66(4)}Ru_{3.34(4)}O_{11}$ chemical compositions, respectively. The results of all the structural data are summarized in Tables I and II. During the Rietveld refinements, Ru was allowed to be in the 2*d* trigonal bipyramid site but this leads to a negative occupation or an occupation inferior to uncertainty, and this 2*d* site was thus considered fully occupied by the 3*d* cation. In some 124 isostructural compounds, a reduction of symmetry from $P6_3/mmc$ to $P6_3/m$ has been observed due to ruthenium pairing in the kagome network [18–20]. Here, neither such phenomenon nor 2*d* sites splitting [13,26], i.e., a reduction of symmetry from $P6_3/mmc$ to $P6_3mc$ due to tetragonal bipyramid splitting to two tetrahedra, has been detected. On the one hand, Table I shows that the 2*a* (*A* site), 6*g,* and 2*d* sites occupancy are relatively similar for the three oxides, within 6% at most. On the other hand, the 4*e* site (face-shared octahedra) occupancy is similar for $Ba_{0.94}Co_{2.43}Ru_{3.57}O_{11}$

TABLE II. Selected interatomic distances (Å) and angles (°) for $A_{1-\delta}M_{2+x}Ru_{4-x}O_{11}$ (A = Ba, Sr and M = Mn, Co, Fe) with uncertainty between parentheses. $M(1)$, $M(2)$, $M(3)$ refers to the M and Ru cations on the 4*e* face-shared octahedra, 6*g* edge-shared octahedra, and 2*d* trigonal bipyramid, respectively.

	$Ba_{0.94}Mn_{2.4}Ru_{3.6}O_{11}$	$Ba_{0.94}Co_{2.4}Ru_{3.6}O_{11}$	$Sr_{0.98}Fe_{2.7}Ru_{3.3}O_{11}$
A–O(1) x 6	2.820(7)	2.783(1)	2.754(1)
A–O(2) x 6	2.95(1)	2.92(2)	2.94(2)
M(1)–O(1) x 3	2.116(8)	1.972(9)	1.917(1)
M(1)–O(2) x 3	2.012(7)	2.022(1)	1.989(1)
M(1)–*M*(1)	2.730(2)	2.659(3)	2.625(3)
M(1)–*M*(2)	3.5716(9)	3.5615(1)	3.5569(1)
M(1)–*M*(3)	3.6634(6)	3.6241(6)	3.6340(8)
O(1)–*M*(1)–O(1)	99.5(5)	99.7(9)	101.0(1)
O(1)–*M*(1)–O(2)	165.5(9)	166.9(6)	165.7(1)
O(1)–*M*(1)–O(2)	89.8(5)	88.6(5)	88.0(8)
O(2)–*M*(1)–O(2)	79.0(7)	81.5(1)	81.2(1)
M(2)–O(1) x 4	1.918(1)	1.998(1)	2.037(1)
M(2)–O(3) x 2	2.071(9)	2.016(1)	2.054(1)
M(2)–*M*(2)	2.9441(1)	2.9199(1)	2.9349(1)
M(2)–*M*(3)	3.7898(1)	3.7667(1)	3.7291(1)
O(1)–*M*(2)–O(1)	87.7(7)	90.0(7)	88.8(7)
O(1)–*M*(2)–O(1)	180.0(1)	180.0(1)	180.0(1)
O(1)–*M*(2)–O(1)	92.3(6)	90.8(8)	91.2(9)
O(1)–*M*(2)–O(3)	95.4(6)	93.4(7)	91.7(7)
O(1)–*M*(2)–O(3)	84.6(7)	86.6(8)	88.3(8)
O(3)–*M*(2)–O(3)	180.0(7)	180.0(9)	180.0(9)
M(3)–O(2) x 3	1.922(1)	1.848(2)	1.894(1)
M(3)–O(3) x 2	2.204(2)	2.262(2)	2.16(2)
O(2)–*M*(3)–O(2)	120.0(1)	120.0(1)	120.0(1)
O(2)–*M*(3)–O(3)	90.0(8)	90.0(1)	90.0(1)
O(3)–*M*(3)–O(3)	180.0(1)	180.0(1)	180.0(1)

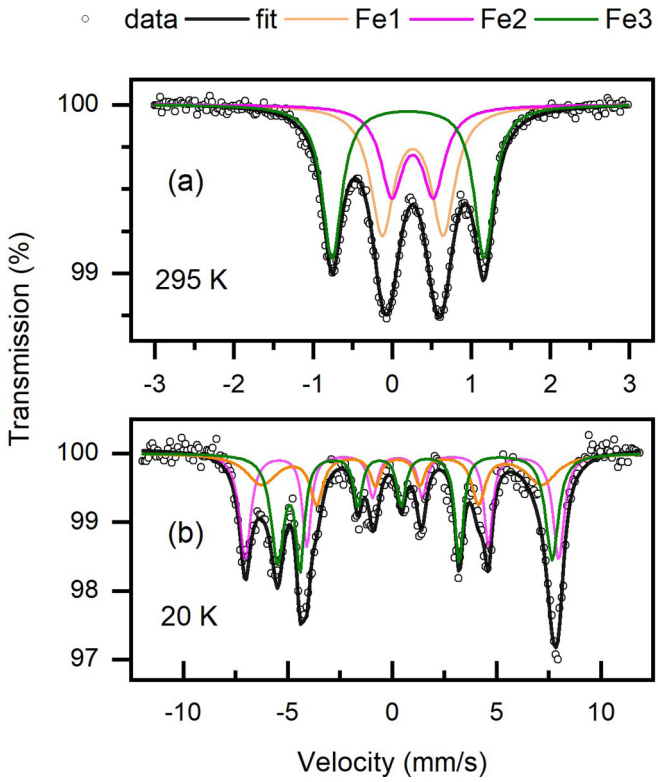


FIG. 4. Mössbauer spectra of $Sr_{0.98}Fe_{2.7}Ru_{3.3}O_{11}$ at 295 K (a) and 20 K (b). The spectra were decomposed into three subspectra corresponding to the Fe1 (orange), Fe2 (pink), and Fe3 (green) sites where the iron cations are positioned.

and $Ba_{0.94}Mn_{2.44}Ru_{3.56}O_{11}$ with 22(2)% and 24(2)% of Co or Mn, and 78(2)% or 76(2)% of Ru, but with an occupancy of 45(1)% for Fe and 55(1)% Ru in $Sr_{0.98}Fe_{2.66}Ru_{3.34}O_{11}$. Another important fact is the A cation deficiency of 0.06 for A = Ba and 0.02 for A = Sr. We highlight that A-site deficiency has not been reported to date. In the following parts, in order to make the reading more comfortable, the three compounds will be referred to as $A_{1-\delta}Mn_{2.4}Ru_{3.6}O_{11}$, $A_{1-\delta}Co_{2.4}Ru_{3.6}O_{11}$, and as $A_{1-\delta}Fe_{2.7}Ru_{3.3}O_{11}$.

For comparison, the Ru metallic sample crystallizes in a hexagonal structure, of the same space group of $P6_3/mmc$ as the 124 ruthenates, and its elementary cell parameters are $a = b = 2.7092(1)$ Å and $c = 4.2887(1)$ Å with a Ru-Ru distance of about 2.67 Å.

B. ^{57}Fe Mössbauer experiments

For $Sr_{1-\delta}Fe_{2.7}Ru_{3.3}O_{11}$, Mössbauer spectrometry was used to investigate in more detail the Fe distribution in the different crystallographic sites and to investigate the Fe nature in this oxide. The Mössbauer spectra of $Sr_{1-\delta}Fe_{2.7}Ru_{3.3}O_{11}$ compound at 295 K (room temperature) and at 20 K (low temperature) are shown in Fig. 4. The room-temperature spectrum shape in the paramagnetic phase contains three overlapping quadrupole doublets, each one associated with a specific Fe site [Fig. 4(a)]. It is important to note that the amount of metallic Fe impurity (0.02 wt.%) deduced from the Rietveld refinement is too small to be detected by Mössbauer spectroscopy, especially since the spectral area of such subspectrum is divided by six in the magnetic state. The accuracy on the measurement of the amount of a given phase is on the order of about 1 to 2%. Therefore, the corresponding subcomponent, if any, would be definitely embedded in the baseline. The doublet with a considerable quadrupole splitting ($\Delta E_Q = 1.91$ mm s^{-1}) corresponds to Fe at the 2d position, as in comparable 4f position in $BaTi_2Fe_4O_{11}$ ($\Delta E_Q = 1.70$ mm s^{-1}) [13]. The relative spectral area of this doublet (38%) is in agreement with full occupation of the 2d site by iron. The additional doublets with smaller quadrupole splitting correspond to the octahedral sites (4e and 6g). These two octahedral sites give a strong overlap of the doublets, and to avoid ambiguous determination of the corresponding hyperfine parameters, the room-temperature spectrum was fitted in a first step by imposing the low-temperature spectral area fractions, and in a second step this parameter was let free. As expected, the spectrum at 20 K [Fig. 4(b)] exhibits well-resolved split lines confirming the development of magnetic ordering and it was fitted by a superposition of three sextets of Lorentzian line shape arising from a combined quadrupolar and magnetic interactions. Line splitting allows one to distinguish more precisely the components (sextets corresponding to the three crystallographic sites), and values of fitted hyperfine parameters and relative spectral area are employed to identify the subspectra and thus to distinguish the various sites (Table III). The 4e, 6g, and 2d site occupancies, derived from the relative spectral areas by assuming the same Lamb-Mössbauer factors, are in good agreement with those obtained by XRD data Rietveld refinements analysis. The room-temperature isomer shift (IS) values lying in the 0.32–0.38-mm s^{-1} range confirm that iron is in high-spin Fe^{3+} state; a lower oxidation state such as Fe^{2+} would give a higher IS value, e.g., above 0.7 mm s^{-1}. The increased measured values at low T are due to the well-known second-order Doppler shift effect. The components attributed to 4e and 6g octahedral sites have the same IS but different ΔE_Q values. At 20 K, the 2d site has a lower hyperfine field than the other sites, and the large value of the quadrupole shift indicates that the magnetic moment is oriented along the principal axis of the electric field gradient which is reported to be the c axis for $SrFe_{3.26}Ru_{2.74}O_{11}$ [28].

C. Magnetic susceptibility

The temperature-dependent magnetic susceptibilities $\chi(T)$ defined as $M(H)/T$ of the three 124 ruthenates are presented in Fig. 5, in 100 Oe for $A_{1-\delta}Mn_{2.4}Ru_{3.6}O_{11}$ and $A_{1-\delta}Co_{2.4}Ru_{3.6}O_{11}$ [Fig. 5(a)], and in 100 Oe [inset of Fig. 5(b)] and 25 kOe for $A_{1-\delta}Fe_{2.7}Ru_{3.3}O_{11}$, this higher magnetic field value being justified by the higher coercive field (see below) [Fig. 5(b)]. In 100 Oe, the zero field cooling (ZFC) and field cooling (FC) curves of $A_{1-\delta}Fe_{2.7}Ru_{3.3}O_{11}$ separate for $T < 280$ K, and the susceptibility measured in larger field presents a broad transition at $T_C \sim 280$ K as a result of this large external field with almost superimposed ZFC and FC curves. This strong 25 kOe applied magnetic field was used for the susceptibility measurement to exceed the much higher coercive field ~20 kOe (Fig. 7). The broadened susceptibility curve for M = Fe is very different from those measured at 100 Oe for M = Co or

TABLE III. Hyperfine parameters and relative spectral area of each component deduced from the fit of the Mössbauer spectra of the $Sr_{0.98}Fe_{2.7}Ru_{3.3}O_{11}$ compound. IS: isomer shift, ΔE_Q: quadrupole splitting, 2ε: quadrupole shift, B_{hf}: hyperfine field.

Temperature (K)	Component	Site	IS (mm s^{-1})	ΔE_Q(mm s^{-1})	2ε(mm s^{-1})	$B_{hf}(T)$	Rel. area (%)	Occ (%)
300	Fe1	4*e*	0.381	0.771			37	48
	Fe2	6*g*	0.380	0.528			25	22
	Fe3	2*d*	0.322	1.919			38	100
20	Fe1	4*e*	0.513		0.205	46.7	34	44
	Fe2	6*g*	0.513		0.197	41.6	27	23
	Fe3	2*d*	0.396		1.685	40.8	39	100

Mn. The $A_{1-\delta}Mn_{2.4}Ru_{3.6}O_{11}$ $\chi(T)$ curve has a maximum around 70 K and the magnetic transition is observed at $T_C = 175$ K. For $A_{1-\delta}Co_{2.4}Ru_{3.6}O_{11}$, the ZFC and the FC curves are separated at low temperature below a transition temperature of 110 K. These susceptibility curves are very close to those previously reported for similar compositions [14,25].

The temperature-dependent inverse magnetic susceptibility $\chi^{-1}(T)$ of these three oxides is shown in Fig. 6 in 100 Oe for $M =$ Co and Mn, and in 25 kOe for $M =$ Fe and are in good agreement with previous reports [14,15,33]. For $A_{1-\delta}Mn_{2.4}Ru_{3.6}O_{11}$ the behavior is close to an ideal Curie-Weiss law with an almost linear increase with temperature from 175 to 400 K. On the other hand, the $\chi^{-1}(T)$ curves of $A_{1-\delta}Co_{2.4}Ru_{3.6}O_{11}$ and $A_{1-\delta}Fe_{2.7}Ru_{3.3}O_{11}$ present a nonlinear behavior, the nonlinearity being more pronounced in the case of $A_{1-\delta}Co_{2.4}Ru_{3.6}O_{11}$, justifying the use of a modified Curie-Weiss behavior $\chi = \chi_0 + \frac{C}{T-\theta_w}$ to fit the data. All the parameters are summarized in Table IV along with the R fit-quality criteria. A quantitative analysis is difficult to achieve given the number of required approximations: number of sites,

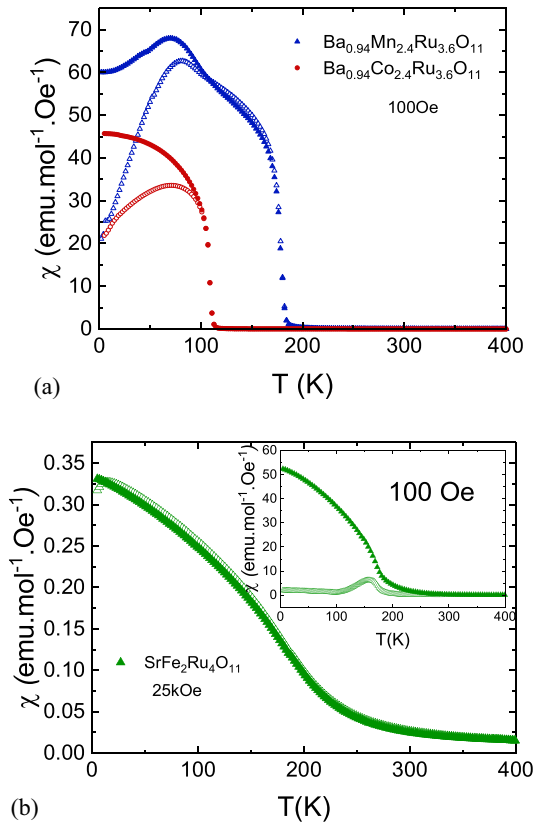


FIG. 5. Temperature-dependent DC magnetic susceptibilities $\chi(T)$ in 100 Oe for $Ba_{0.94}Co_{2.4}Ru_{3.6}O_{11}$ and $Ba_{0.94}Mn_{2.4}Ru_{3.6}O_{11}$ (a) and in 25 kOe (b) and 100 Oe for $Sr_{0.98}Fe_{2.7}Ru_{3.3}O_{11}$ (inset of b). Empty symbols correspond to the ZFC curves and the full ones to FC curves.

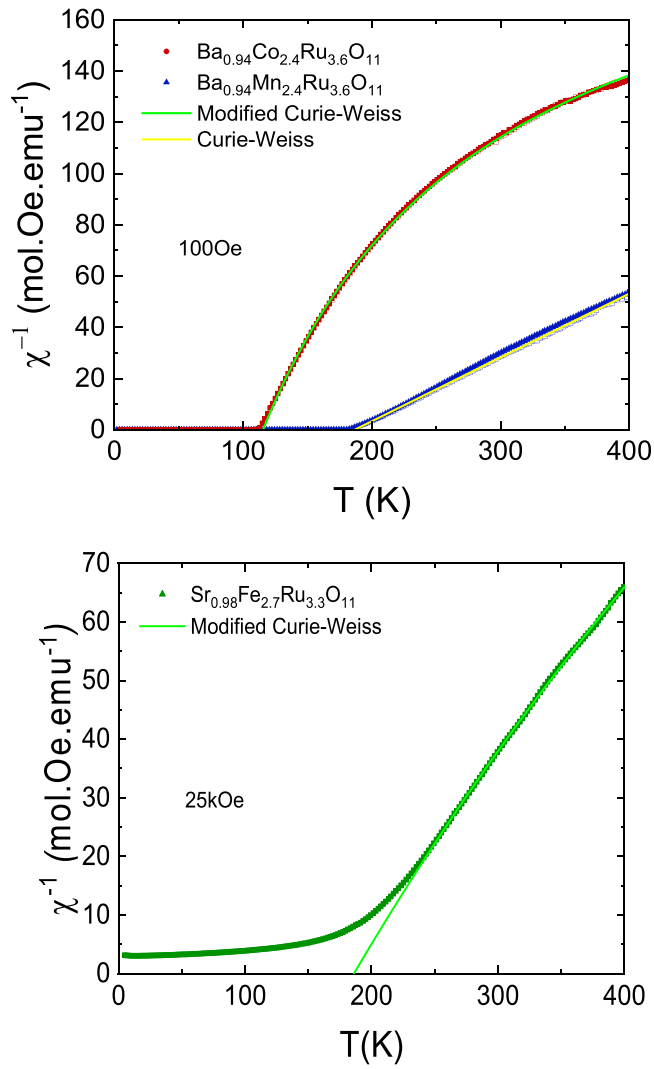


FIG. 6. Temperature-dependent inverse DC magnetic $\chi^{-1}(T)$ in 100 Oe for $Ba_{0.94}Co_{2.4}Ru_{3.6}O_{11}$ and $Ba_{0.94}Mn_{2.4}Ru_{3.6}O_{11}$ (a) and in 25 kOe for $Sr_{0.98}Fe_{2.7}Ru_{3.3}O_{11}$ (b), with the Curie-Weiss fitting (parameters are given in Table IV).

TABLE IV. Parameters extracted from Curie-Weiss fit for $Ba_{0.94}Mn_{2.4}Ru_{3.6}O_{11}$ and from modified-Curie Weiss fit for $Ba_{0.94}Co_{2.4}Ru_{3.6}O_{11}$ and $Sr_{0.98}Fe_{2.7}Ru_{3.3}O_{11}$ with uncertainty between parentheses.

	C(K mol Oe emu^{-1})	$\mu_{\text{eff}}(\mu_B$/f.u.)	θ_w(K)	χ_0(emu mol^{-1} Oe^{-1})	R
$Ba_{0.94}Mn_{2.4}Ru_{3.6}O_{11}$	4.014(6)	5.67	186.2(7)		0.999 72
$Ba_{0.94}Co_{2.4}Ru_{3.6}O_{11}$	0.802(3)	2.53	115.4(2)	$4.4(2)\times10^{-3}$	0.999 71
$Sr_{0.98}Fe_{2.7}Ru_{3.3}O_{11}$	2.72(3)	4.67	186.1(8)	$2.5(1)\times10^{-3}$	0.999 78

M/Ru ratio at each site, valence state and spin configuration of each cation at each site [14,15,33]. Still, the measurement of $\chi(T)$ for M = Fe is interesting as previous studies on several Fe/Ru ratios either in single-crystalline or polycrystalline sample showed a linearity between T_C value and Fe content [16,25]. Following that empirical fact, the $T \sim 280$ K value extracted from the $\chi^{-1}(T)$ inflexion point (Fig. 6), consistent with the T_{kink} on the T-dependent resistivity curve (Fig. 8), leads to an Fe content of $43 \pm 5\%$, which is in good agreement with the extracted one from the Rietveld refinement analysis, i.e., $44 \pm 2\%$, confirming our structural analysis.

The field-dependent magnetization at 5 K is shown in Fig. 7. The magnetization for M = Co, Mn exhibits very small hysteresis with strong magnetization increase at low field, reaching 1.5 and 5 μ_B/f.u. at 50 kOe, respectively, without saturation up to 140 kOe (Fig. 7 left inset). Unlike these two oxides, $A_{1-\delta}Fe_{2.7}Ru_{3.3}O_{11}$ has a broad hysteresis, with M reaching 2.9 μ_B/f.u. at 50 kOe. The coercive fields are very small for $A_{1-\delta}Co_{2.4}Ru_{3.6}O_{11}$ and $A_{1-\delta}Mn_{2.4}Ru_{3.6}O_{11}$, close to 100 Oe, determined from the low-field magnetization curves (Fig. 7 right inset). These small values are in strong contrast with the large coercive field H_C = 19 kOe for $A_{1-\delta}Fe_{2.7}Ru_{3.3}O_{11}$, characteristic of "hard ferromagnetism" resulting from its ferrimagnetism [28]. Such a large value close to 20 kOe is remarkable, being more than twice than the one of $BaFe_{12}O_{19}$ M-type hexaferrite at the same T [34]. To conclude, these hexagonal ruthenates are all ferrimagnetic but characterized by different T_Cs, saturated magnetizations, and coercive fields.

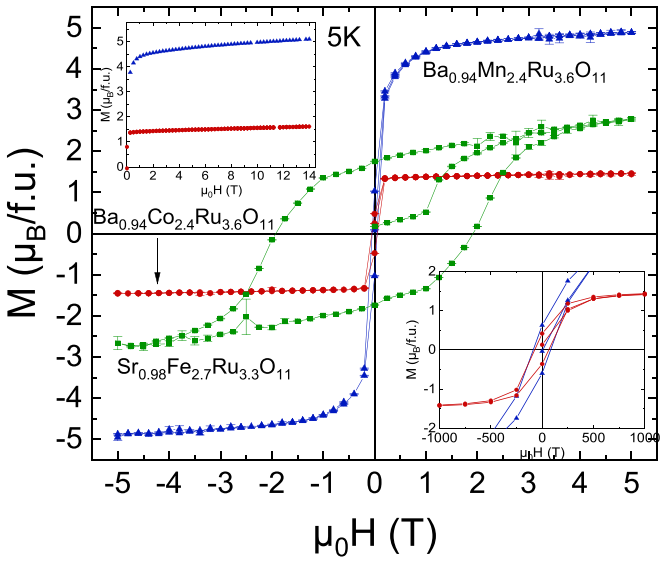


FIG. 7. Field-dependent magnetization at 5 K with, for Mn- (blue), Co- (red), and Fe- (green) 124 oxides, low-field magnetization (lower inset) and high-field magnetization up to 14 T (upper inset).

D. Transport properties

1. Electrical resistivity

The temperature-dependent resistivities of the three oxides are shown in Fig. 8, measured up to 600 K. Despite their polycrystalline nature, they all exhibit small values of resistivity close to 2–15 mΩ cm from 2 to 600 K, with a clear evolution from metallicity for M = Co to a more localized behavior for M = Fe. These results obtained on polycrystals are in good agreement with the previous measurements of single crystals with A = Ba [15]. The resistivity of $A_{1-\delta}Co_{2.4}Ru_{3.6}O_{11}$ is the smallest one, with values on the order of ∼2 mΩ cm and only a small temperature dependence. An anomaly is clearly seen at T_C, also visible in the first derivative curve (inset of Fig. 8), followed by a maximum and a sign change of the slope around 350 K. Also, a small ρ increase is observed at low temperature. $A_{1-\delta}Mn_{2.4}Ru_{3.6}O_{11}$ resistivity is on the order of ∼5 mΩ cm and presents a very weak T dependence. Contrary to $A_{1-\delta}Co_{2.4}Ru_{3.6}O_{11}$, the $d\rho/dT$ slope is negative in the whole T range. It presents a kink at T_C, observed on the $d\rho/dT$ curve (inset of Fig. 8). $A_{1-\delta}Fe_{2.7}Ru_{3.3}O_{11}$ behaves like a semiconductor ($d\rho/dT < 0$), but with a relatively weak low-temperature localization with values on the order of ∼15 mΩ cm at 5 K. Like the two others, it has an anomaly at T_C (inset of Fig. 8).

A change of regime is observed around 350 K for $A_{1-\delta}Co_{2.4}Ru_{3.6}O_{11}$ compound, with a ρ maximum reaching

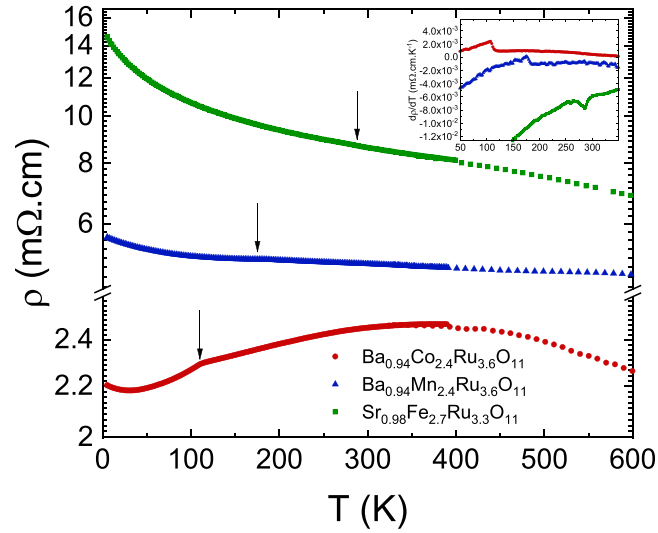


FIG. 8. Temperature-dependent resistivity. Arrows denotes the magnetic transitions. Inset: $d\rho/dT$ curves.

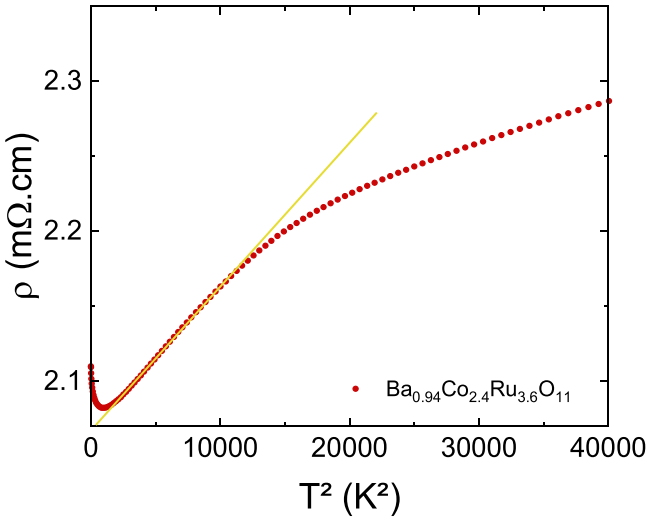


FIG. 9. T^2-dependent resistivity of $Ba_{0.94}Co_{2.4}Ru_{3.6}O_{11}$. Also shown is the linear fit (yellow) to the data in the range 50 to 90 K.

2.4 mΩ cm. This contrasts with the nonsaturating behavior observed in the ferromagnetic and metallic $SrRuO_3$, a well-known example of bad metallic behavior. This maximum of resistivity can generally be interpreted using the Mott Ioffe Regel limit which implies that the mean-free path cannot be smaller than the typical unit-cell parameter, this criterion defining the Mott Ioffe Regel temperature T_{MIR}. This point will be discussed later.

A T^2 behavior is observed at $T < T_C$ at relatively high temperature, between 50 and 90 K, following $\rho = AT^2 + \rho_0$ with $A = 9.95(2)10^{-9}\Omega$ cm K^{-2} and $\rho_0 = 2.11(1)\Omega$ cm as shown in Fig. 9. In Ref. [16], the Sommerfeld coefficient of nominal $BaCo_2Ru_4O_{11}$ composition was reported, $\gamma = 120$ mJ mol^{-1} K^{-2}. The Kadowaki-Woods ratio would thus be $A/\gamma^2 = 0.67\mu\Omega$ cm mol^2 K^2 J^2, a value very close to the pure transition metals one ~ 0.4 $\mu\Omega$ cm mol^2 K^2 J^{-2}, and ~ 25 times smaller than the empirical value expected for a correlated system (10 $\mu\Omega$ cm mol^2 K^2 J^{-2}) [35], showing again the major difference with the $SrRuO_3$ oxide for which the Kadowaki-Woods ratio reaches $\sim$6–15 $\mu\Omega$ cm mol^2 K^2 J^{-2} [36,37].

2. Magnetoresistance

In the three samples, the influence of magnetic transitions does not have a strong impact on the resistivity but is nevertheless visible by kinks around their respective T_{Cs} as shown in the inset of Fig. 8. For M = Fe, the kink is observed at 288 K, in good agreement with the transition observed in the magnetic susceptibility at $T \sim 280$ K. To further investigate the possible impact of magnetism on transport, the magnetoresistance (MR) curves have been analyzed. The results are presented in Fig. 10, with first the evolution of the magnitude of MR in 9 T as a function of temperature [Fig. 10(a)], and in Fig. 10(b), the MR curves versus magnetic field for M = Co, Mn, and Fe. All the MR curves are negative, with very small values (except for very small and positive values for M = Fe around $T \sim$ 100–200 K). The maximum MR is observed for M = Mn at 5 K, reaching -1%. It must be noted that the polycrystalline nature should enhance MR properties

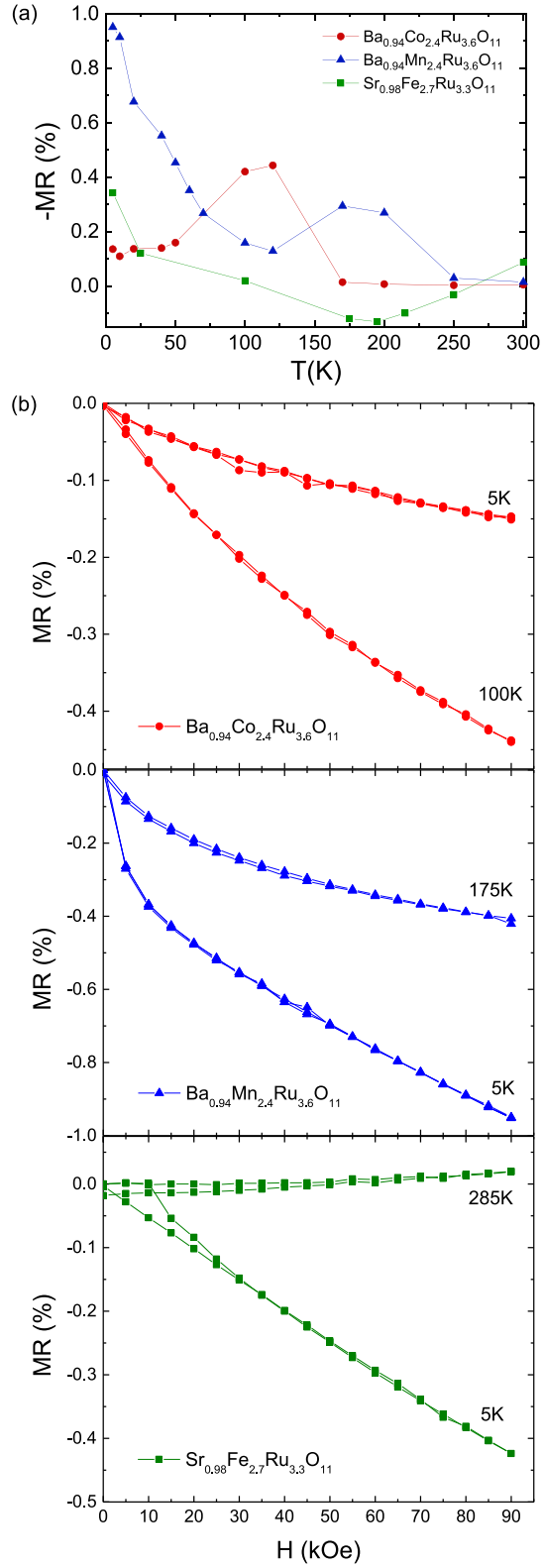


FIG. 10. (a) (-MR) of Co-, Mn-, and Fe-124 oxides as a function of temperature at 9 T with MR defined as $100 \times [(\rho(H) - \rho(0))/\rho(0)]$, and MR as a function of magnetic field in (b).

via tunneling at the grain boundaries [38], thus confirming that MR data are intrinsically small in $A_{1-\delta}M_{2+x}Ru_{4-x}O_{11}$. This is much smaller than the ones of $SrRuO_3$ measured in thin films [39], close to -6 to -10%, or than the ones of CrO_2

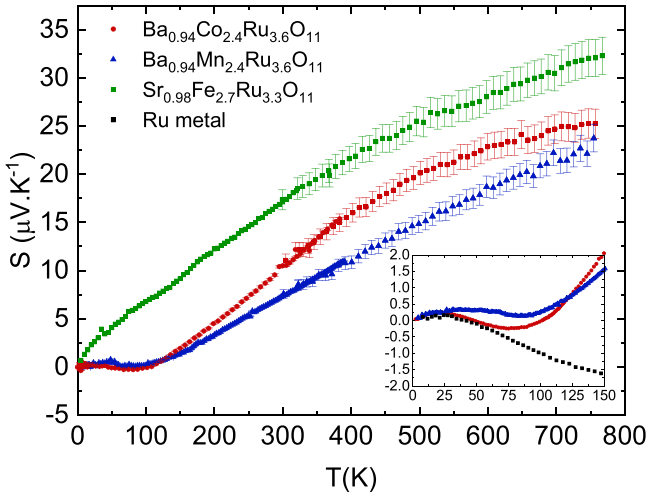


FIG. 11. Temperature-dependent Seebeck coefficient. Inset: low-temperature $S(T)$ of Co-, and Mn- 124 oxides and Ru metal, from 8 to 150 K.

another example of ferromagnetic oxides with spin-polarized transport for which MR reaches up to +25% at 5 K [38,40]. This is also much smaller than the MR measured in the ferrimagnetic Sr_2FeMoO_6 double perovskites which exhibit similar values of electrical resistivities, with MR reaching up to −42% in 7 T at 4.2 K [41].

The evolution of MR with T presented in Fig. 10(a) shows that MR continuously decreases as a function of temperature, except around T_C where a maximum is observed for M = Co and M = Mn. At low T, the high-field MR values follow the magnetization behavior M, with MR the largest for M = Mn. At 5 K and 5 T, the comparison with Fig. 7 shows that these MR values follow the evolution of magnetization M and moreover reflect the evolution of the M^2 behavior, with MR $\sim M^2$, i.e., MR(M = Mn)/MR(M = Fe) = 3, similar to the ratio $M^2(M = \text{Mn})/M^2(M = \text{Fe})$, while these ratios reach close values respectively, 2.5 and 3.5, for the comparison between Fe and Co. This low-temperature M^2 behavior is typically observed in the presence of spin-polarized tunneling at grain boundaries as in manganites [42] or in $SrRuO_3$ [38] and most probably reflects the polycrystalline nature of the samples. Consistently, the $M(H)$ and MR(H) curves are interrelated, as the MR curves are reversible for M = Co, Mn, but display hysteresis below ∼25 kOe for M = Fe, in good agreement with the large coercive field measured on the $M(H)$ loops (Fig. 7). It is interesting to note that three different behaviors are observed depending on the transition-metal cation M, with a maximum of MR observed around T_C for M = Co, a maximum at 5 K observed for M = Mn together with a secondary maximum around T_C, and finally only very small values for M = Fe and no peak around T_C. The coupling between magnetism and transport at T_C is therefore maximum for M = Co.

3. Thermopower

The temperature-dependent Seebeck coefficients $S(T)$ of the three samples are presented in Fig. 11. In $A_{1-\delta}Mn_{2.4}Ru_{3.6}O_{11}$, $S(T)$ is linear and positive from ∼100 to 750 K, reaching ∼22.5 μV K^{-1}. At T < 100 K, S is very close to 0μV K^{-1}, as for M = Co presented in the inset. At T > 100 K in $A_{1-\delta}Co_{2.4}Ru_{3.6}O_{11}$, S is linear up to about 350 K then diverges from this linearity to reach ∼25μV K^{-1} at 750 K. For these two compounds, the slopes of $S(T)$ above 100 K are equal to 0.0375 μV K^{-2} for M = Mn and 0.0551 μV K^{-2} for M = Co. Using the classical Boltzmann equation for S would lead to an equivalent Fermi energy of 7500 K for M = Mn and 5000 K for M = Co, suggesting a large bandwidth for both ruthenates. Unlike the two other compounds, the Seebeck coefficient of $A_{1-\delta}Fe_{2.7}Ru_{3.3}O_{11}$ is not close to 0 μV K^{-1} at T < 100 K but increases on the whole temperature range, reaching 32.5 μV K^{-1} at 750 K.

From the crude estimation of an "effective" Fermi energy of 5000 K for M = Co, the analysis of the Mott Ioffe Regel limit previously discussed can be made using the formula $\rho_{MIR} \sim \frac{3\pi h}{2\pi(e^2 k_F^2 d)}$. The value of ρ_{MIR} = 2.5 mΩ cm for M = Co (Fig. 8) corresponds to $d \sim 0.16$ nm, using an effective mass of $m = m_0$ and a very simple spherical Fermi surface. Considering the crude assumptions made for this analysis, this d value seems reasonable especially if one compares to the a unit-cell parameter value, $a \approx 0.6$ nm, confirming that for M = Co, the transport properties can be described as a metal with a large Fermi energy.

The Seebeck coefficients of $BaCo_{2+x}Ru_{4-x}O_{11}$, with x = 0 and 0.5, have been reported previously in the range of temperature 80 K < T < 450 K [32], and our values are very close to theirs within ±2 μV K^{-1} at 100 K. In all three samples, positive S values would suggest holes as majority charge carriers in the unlikely case of a simple spherical Fermi surface, in contrast to Hall effect measurement in a M = Co 124 ferrite showing a Hall coefficient associated with electrons [21]. As thermopower is a measurement technique less sensitive to grain boundaries than the resistivity, the lack of anomaly observed at T_C, unlike in $SrRuO_3$, confirms the moderate impact if any of the spin ordering in the T_C region on S. Also, the transition between the metallic state of $A_{1-\delta}Co_{2.4}Ru_{3.6}O_{11}$ to the more localized state of $A_{1-\delta}Fe_{2.7}Ru_{3.3}O_{11}$ does not have a strong impact on the Seebeck coefficient. The three thermopower curves only display small differences, especially for M = Co and M = Mn, compared to the large differences observed on $\chi(T)$ and $\rho(T)$ curves in the whole T range, as if the M cation has no impact. Values are slightly higher in the case of $A_{1-\delta}Fe_{2.7}Ru_{3.3}O_{11}$ all along the temperature range, for which ρ is slightly higher, but the Seebeck value differences remain low. For $A_{1-\delta}Mn_{2.4}Ru_{3.6}O_{11}$ and $A_{1-\delta}Co_{2.4}Ru_{3.6}O_{11}$, the $S(T)$ evolutions do not reproduce the same evolution as ρ: S is larger in $A_{1-\delta}Co_{2.4}Ru_{3.6}O_{11}$ which is the most metallic compound. Considering the complexity of the band structure, only a complete calculation taking into account the carriers concentration and their mobility could explain this, and give a correct S estimate.

Though the thermopower in the T_C region and below appears rather classical as Boltzmann equation is used, the high-T S value is characteristic of the ones previously measured in stoichiometric $SrRuO_3$, in substituted and non-stoichiometric $SrRuO_3$, in quadruple perovskites [8,9] and more recently observed in hollandites with Ru in octahedral sites (with a mixed occupation by Cr and Ru) [10]. This value was attributed to spin entropy induced by the ruthenium cations, with a mixed valency Ru^{3+}/Ru^{4+} or Ru^{4+}/Ru^{5+} [8].

For the latter case, the thermopower was written

$$S = \frac{k_B}{e}\left[\ln\left(\frac{x}{1-x}\right)\right] + \frac{k_B}{e}\left[\ln\left(\frac{D(d^4)}{D(d^5)}\right)\right], \qquad (1)$$

where $D(d^4)$ [$D(d^5)$] is the spin-only degeneracy of Ru^{4+} (Ru^{3+}), with $D(d^4) = 3(S = 1)$ and $D(d^5) = 2(S = 3/2)$. In Eq. (1), the first term corresponds to the transport functions and the second one to the entropic one [43]. The entropic part of thermopower is often known as the generalized Heikes formula, and is the high-T limit of thermopower, reached as soon as the transport term becomes negligible. This entropic term depends on the doping and on the spin and orbital degeneracies of the transition-metal cation in case of cobaltites, chromium oxides, or ruthenates [44,45]. For this latter case, an exact calculation based on local density approximation+dynamical mean field theory (LDA+DMFT) of the thermopower has been performed for Sr_2RuO_4 [12] with Ru^{4+}, which gave for the high-T limit $S = (k_B/2e)[\ln(D(d^3)/D(d^5))] = (k_B/2e)\ln 2 \approx 30\,\mu V\ K^{-1}$. In this expression, the transport term of Eq. (1) is suppressed avoiding the expected but not experimentally observed S divergence near stoichiometric Ru^{4+} ($x = 0$). This $(k_B/2e)\ln 2$ value comes thus from the ruthenates Hund's metal features with fluctuating spins and quenched orbitals. Remarkably enough, even if very different band structures as compared to square-lattice ruthenates are formed in the present three hexagonal oxides as evidenced by resistivity measurements and by low-T Seebeck coefficient measurements, the transport term associated with these band structures seems also to be negligible, leading to similar values at ~700 K, close to $\approx 30\,\mu V\ K^{-1}$, strongly supporting a spin entropy-dominated thermopower as in the case of Sr_2RuO_4 [12,43].

4. Comparison of the thermopower of $A_{1-\delta}M_{2+x}Ru_{4-x}O_{11}$ with the Ru thermopower

One uncommon feature is that at low T, S tends to reach very small values close to zero in these two compounds in a large T range, below 100 K, in contrast to $A_{1-\delta}Fe_{2.7}Ru_{3.3}O_{11}$. Also, for $A_{1-\delta}Co_{2.4}Ru_{3.6}O_{11}$, S is not proportional to the Sommerfeld coefficient as T tends to 0 K unlike many oxides and so, with $q = SN_{av}e/T\gamma = 0.014$, it does not match with the Behnia-Jaccard-Floquet universal line of $S/T = f(\gamma)$ [46], keeping in mind the only available gamma value is for $BaCo_2Ru_4O_{11}$. The T range close to $0\,\mu V\ K^{-1}$ corresponds to ~$0.91T_C$ and ~$0.56T_C$ for $A_{1-\delta}Co_{2.4}Ru_{3.6}O_{11}$ and $A_{1-\delta}Mn_{2.4}Ru_{3.6}O_{11}$, respectively, and thus does not correspond to a precise ratio of T/T_C. This very small value of S could be due to a compensation effect between different carriers. Nevertheless, given the very low values typical of metal, this could also be a sign of metallic conduction through the ruthenium network. As shown in Table II, the $M(1)$-$M(1)$ (dimers of face-shared octahedra) and $M(2)$-$M(2)$ (kagome lattice) distances determined at 300 K are very small, reaching ~2.625 to 2.730 Å for $M(1)$-$M(1)$ and 2.920 to 2.944 Å for $M(2)$-$M(2)$ depending on M. In metallic Ru, the Ru-Ru distances are equal to 2.67 Å, very close to the ones determined for $M(1)$-$M(1)$. Thus, at low T, there might be direct pathways between Ru-Ru orbitals rather than through Ru-O orbitals only [47]. The edge-shared octahedra in the kagome layers and the corner-shared connections between these layers and the dimers would ensure delocalization throughout the structure. To the best of our knowledge, no low-T (<80 K) Seebeck coefficient of Ru metal has been published so far. Hence, the ruthenium metal Seebeck coefficient was measured in the range 8 K < T < 150 K and compared with those of $A_{1-\delta}Co_{2.4}Ru_{3.6}O_{11}$ and $A_{1-\delta}Mn_{2.4}Ru_{3.6}O_{11}$, as shown in the inset of Fig. 11. The values at 100 K are very close to the ones previously reported [48]. Intriguingly, very similar behaviors below 50 K are observed for Ru metal and $A_{1-\delta}Co_{2.4}Ru_{3.6}O_{11}$, with a maximum around 25 K. The three Seebeck coefficients, with the one of $A_{1-\delta}Mn_{2.4}Ru_{3.6}O_{11}$, are superimposed for T < 25 K. This is in favor of the existence of direct metallic paths at low temperature [47]. The presence of such short Ru-Ru distances is however not a sufficient condition, as S does not tend to metallic Ru values in the case of $A_{1-\delta}Fe_{2.7}Ru_{3.3}O_{11}$. But for M = Fe, other parameters could justify this difference, as the richer M content of 45% in the face-shared octahedra reduces the number of Ru(1)-Ru(1) dimers. Finally, it should be noted that such very small metallic values could be affected by possible phonon drag effect or could be modified by disorder effect as in standard metals. The phonon drag effect should be strongly decreased due to the polycrystalline nature of the samples [49], and understanding a possible phonon drag or disorder effect would require the investigation of several samples with different degrees of disorder, which is beyond the scope of the present paper.

IV. DISCUSSION AND CONCLUDING REMARKS

In the 124 ruthenates family, $A_{1-\delta}Co_{2.4}Ru_{3.6}O_{11}$, $A_{1-\delta}Mn_{2.4}Ru_{3.6}O_{11}$, and $A_{1-\delta}Fe_{2.7}Ru_{3.3}O_{11}$ show an interesting evolution of the resistivity, from metallic behavior ($d\rho/dT > 0$), to a negative value of $d\rho/dT$. The electrical resistivities are in the mΩ cm range and the T dependences of the Seebeck coefficients are consistent with this metallic behavior. Even if the nature of the M cation strongly modifies the magnetic properties, the effect of magnetic ordering is slightly visible only as anomaly on the $\rho(T)$ curves, and not observed on the $S(T)$ curves.

In the high-T limit, the Seebeck coefficient tends to reach in all three compounds the ruthenium oxides characteristic values near $30\,\mu V\ K^{-1}$ (at 750 K, $25\,\mu V\ K^{-1}$ for M = Mn, Co and $32.5\,\mu V\ K^{-1}$ for M = Fe). This high-T value characteristic of ruthenates supports the fact that transport is dominated by the Ru orbitals rather than those of the M magnetic cations. The more localized behavior observed for M = Fe also suggests that the 4*e* site (face-shared octahedra) plays an important role in the electronic transport as the Ru content in these dimers is smaller for M = Fe than for M = Co or Mn. Detailed band-structure calculations are necessary to explain the respective role of Ru in the kagome layers and their connections through these dimers, both entities showing shorter Ru-Ru distances as compared to perovskite-derived ruthenates.

As T decreases, a transition from an entropy-dominated Seebeck coefficient to unprecedented very small metal-like Seebeck coefficient is observed for M = Co and M = Mn. In particular, below 100 K, the $S \sim 0\,\mu V\ K^{-1}$ values similar to those of Ru metal point towards an original mechanism of

Ru-Ru metallic direct exchange associated with the presence of short Ru-Ru distance.

ACKNOWLEDGMENTS

The authors thank Dr. David Berthebaud for Ru metal shaping, Dr. Igor Mazin (George Mason University) and Dr. Jernej Mravlje (Jozef Stefan Institute, Ljubljana University) for stimulating discussions. The authors are grateful to X. Larose and Dr. S. Gascoin for the technical support in TEM and x-ray-diffraction measurements respectively, and F. Veillon for his assistance in susceptibility and transport measurements. This work was partly supported by Région Normandie through the RIN TEMPO project.

[1] Y. Maeno, H. Hasimoto, K. Yoshida, S. Nishizaki, T. Fujita, J. G. Bednorz, and F. Lichtenberg, Nature (London) **372**, 532 (1994).
[2] P. Steffens, Y. Sidis, J. Kulda, Z. Q. Mao, Y. Maeno, I. I. Mazin, and M. Braden, Phys. Rev. Lett. **122**, 047004 (2019).
[3] H. Mukuda, K. Ishida, Y. Kitaoka, K. Asayama, R. Kanno, and M. Takano, Phys. Rev. B **60**, 12279 (1999).
[4] V. Hardy, B. Raveau, R. Retoux, N. Barrier, and A. Maignan, Phys. Rev. B **73**, 094418 (2006).
[5] Y. Liu, H. P. Nair, J. P. Ruf, D. G. Schlom, and K. M. Shen, Phys. Rev. B **98**, 041110 (2018).
[6] S. Kunkemöller, K. Jenni, D. Gorkov, A. Stunault, S. Streltsov, and M. Braden, Phys. Rev. B **100**, 054413 (2019).
[7] H. Yoshino, K. Murata, N. Shirakawa, Y. Nishihara, Y. Maeno, and T. Fujita, J. Phys. Soc. Jpn. **65**, 1548 (1996).
[8] Y. Klein, S. Hébert, S. Kolesnik, T. Maxwell, B. Dabrowski, and A. Maignan, Phys. Rev. B. **73**, 052412 (2006).
[9] S. Hébert, R. Daou, and A. Maignan, Phys. Rev. B **91**, 045106 (2015).
[10] F. Pawula, S. Hébert, D. Pelloquin, and A. Maignan, J. Mater. Chem. C **7**, 86 (2019).
[11] X. Deng, K. Haule, and G. Kotliar, Phys. Rev. Lett. **116**, 256401 (2016).
[12] J. Mravlje and A. Georges, Phys. Rev. Lett. **117**, 036401 (2016).
[13] M. C. Cadée and D. J. W. Ijdo, J. Solid State Chem. **52**, 302 (1984).
[14] M. L. Foo, Q. Huang, J. W. Lynn, W.-L. Lee, T. Klimczuk, I. S. Hagemanna, N. P. Ong, and R. J. Cava, J. Solid State Chem. **179**, 563 (2006).
[15] B. Schüpp-Niewa, L. Shlyk, S. Kryukov, L. E. De Long, and R. Niewa, Z. Naturforsch. **62b**, 753 (2007).
[16] R. Niewa, L. Shlyk, B. Schüpp-Niewa, and L. E. De Long, Z. Anorg. Allg. Chem. **636**, 331 (2010).
[17] S. Nemrava, L. Link, Z. Hu, B. Blaschkowski, S.-C. Liao, H.-J. Lin, C.-T. Chen, T.-S. Chan, L. H. Tjeng, and R. Niewa, Z. Anorg. Allg. Chem. **644**, 1691 (2018).
[18] L. Shlyk, S. Strobel, E. Rose, and R. Niewa, Solid State Sci. **14**, 281 (2012).
[19] L. Shlyk, S. Strobel, T. Schleid, and R. Niewa, Z. Kristallogr. **227**, 545 (2012).
[20] L. Shlyk, L. E. De Long, and R. Niewa, Phys. Rev. B. **95**, 024433 (2017).
[21] Y. Kanke, Phys. Rev. B **60**, 3764 (1999).
[22] H. Kato, M. Kato, K. Yoshimura, and K. Kosuge, J. Phys.: Condens. Matter **13**, 9311 (2001).
[23] D. Verdoes, H. W. Zandbergen, and D. J. W. Ijdo, Mater. Res. Bull. **22**(1987).
[24] L. Shlyk, L. E. De Long, S. Kryukov, B. Schüpp-Niewa, and R. Niewa, J. Appl. Phys. **103**, 07D112 (2008).
[25] L. Shlyk, S. Kryukov, B. Schüpp-Niewa, R. Niewa, and L. E. De Long, Adv. Mater. **20**, 1315 (2008).
[26] I. D. Posen, T. M. McQueen, A. J. Williams, D. V. West, Q. Huang, and R. J. Cava, Phys. Rev. B. **81**, 134413 (2010).
[27] L. Shlyk, R. Niewa, and L. E. De Long, Phys. Rev. B **82**, 134432 (2010).
[28] L. Shlyk, B. G. Ueland, J. W. Lynn, Q. Huang, L. E. De Long, and S. Parkin, Phys. Rev. B **81**, 184415 (2010).
[29] T. Roisnel and J. Rodríguez-Carvajal, Materials Science Forum, Proceedings of the European Powder Diffraction Conference (EPDIC7) **378**, 118 (2001).
[30] P. A. Stadelmann, Ultramicroscopy **21**, 131 (1987).
[31] E. Mun, S. L. Bud'ko, M. S. Torikachvili, and P. C. Canfield, Meas. Sci. Technol. **21**, 055104 (2010).
[32] B. Pato-Doldan, M. Sanchez-Andujar, S. Castro-Garcia, and M. A. Senaris-Rodriguez, J. Alloys Compd. **509**, 1529 (2011).
[33] L. Shlyk, S. Parkin, and L. E. De Long, Phys. Rev. B **81**, 014413 (2010).
[34] P. Shepherd, K. K. Mallick, and R. J. Green, J. Magn. Magn. Mater. **311**, 683 (2007).
[35] A. C. Jacko, J. O. Fjærestad, and B. J. Powell, Nat. Phys. **5**, 422 (2009).
[36] O. Morán, W. Saldarriaga, and E. Baca, Superlatt. Microstruct. **55**, 151 (2013).
[37] N. Kikugawa, R. Baumbach, J. S. Brooks, T. Terashima, S. Uji, and Y. Maeno, Cryst. Growth, Des. **15**, 5573 (2015).
[38] M. S. Anwar and J. Aarts, Phys. Rev. B **88**, 085123 (2013).
[39] L. Klein, A. F. Marshall, J. W. Reiner, C. H. Ahn, T. H. Geballe, M. R. Beasley, and A. Kapitulnik, J. Magn. Magn. Mater. **188**, 319 (1998).
[40] Y. Kats, L. Klein, J. W. Reiner, T. H. Geballe, M. R. Beasley, and A. Kapitulnik, Phys. Rev. B **63**, 054435 (2001).
[41] K.-I. Kobayashi, T. Kimura, H. Sawada, K. Terakura, and Y. Tokura, Nature (London) **395**, 677 (1998).
[42] M. Viret, L. Ranno, and J. M. D. Coey, J. Appl. Phys. **81**, 4964 (1997).
[43] M. R. Peterson and S. B. Shastry, Phys. Rev. B **82**, 195105 (2010).
[44] J-P. Doumerc, J. Solid State Chem. **110**, 419 (1994).
[45] W. Koshibae, K. Tsutsui, and S. Maekawa, Phys. Rev. B **62**, 6869 (2000).
[46] K. Behnia, D. Jaccard, and J. Flouquet, J. Phys.: Condens. Matter **16**, 5187 (2004).
[47] J. B. Goodenough, Phys. Rev. **117**, 1442 (1960).
[48] *CRC Handbook of Thermoelectrics*, edited by D. M. Rowe (CRC Press, Boca Raton, FL, 1995).
[49] H. Takahashi, R. Okazaki, S. Ishiwata, and H. Taniguchi, Nat. Commun., **7**, 12732 (2016).